Article

A Hybrid Energy Storage System Integrated with a Wave Energy Converter: Data-Driven Stochastic Power Management for Output Power Smoothing

Dario Pelosi [1], Federico Gallorini [2], Giacomo Alessandri [2] and Linda Barelli [1,*]

[1] Department of Engineering, University of Perugia, Via G. Duranti 93, 06125 Perugia, Italy; dario.pelosi@unipg.it

[2] VGA srl, Via Ugo Foscolo 1, 06053 Deruta, Italy; federico.gallorini@vgasrl.com (F.G.); giacomo.alessandri@vgasrl.com (G.A.)

[*] Correspondence: linda.barelli@unipg.it

Abstract: Beyond solar and wind energy, wave energy is gaining great interest due to its very high theoretical potential, although its stochastic nature causes intermittent and fluctuating power production. Energy storage system (ESS) integration to wave energy converter (WEC) plants represents a promising solution to mitigate this issue. To overcome the technological limits of the single storage devices, the hybridization of complementary ESSs represents an effective solution, extending the operating range over different timeframes. This paper analyzes the benefits of Li-ion battery–supercapacitor hybrid ESS integration into a grid-connected WEC, aiming at smoothing the produced power oscillations. The hybridization concept involves coupling a power-intensive technology, such as a supercapacitor devoted to managing fluctuations at higher frequency, with a battery technology exploited to manage power variations over longer timeframes to mitigate degradation issues. In this study, a multi-objective data-driven power management strategy, based on the simultaneous perturbation stochastic approximation (SPSA) algorithm, is implemented to minimize power fluctuations in terms of power ramp (representing the power variation between two consecutive values with a 1 s time step), both at the Point of Common Coupling (PCC) and the Li-ion battery terminals, thanks to the supercapacitor peak-shaving function. The SPSA management strategy, together with a suitable sizing procedure, allows a reduction of more than 70% in the power oscillations at the PCC with respect to those at the WEC terminals, while decreasing battery stress by more than 25% if compared to a non-hybrid ESS consisting of a Li-ion battery. This shows how supercapacitor features can extend battery lifespan when integrated in a hybrid ESS.

Keywords: stochastic power management; battery; supercapacitor; power smoothing; renewables

1. Introduction

Research on energy production is investigating new frontiers to generate electricity with no emissions to face climate change. The exploitation of zero-emission sources such as renewable energy sources (RESs) is intensively investigated since RESs produce no carbon dioxide or pollutant emissions and are largely available all over the world. Beyond solar and wind energy, energy from waves is gaining great interest due to its very high theoretical potential (29,500 TWh/year) [1,2]. Nevertheless, RESs' stochastic nature causes intermittent and fluctuating power production because of the variation in meteorological conditions. This non-programmability yields issues with grid stability and safety, necessitating an improvement in system reliability, load management, and power quality [3]. Such aspects should be quickly addressed because of the expected rapid increase in RES installed capacity. Indeed, the grid needs to manage higher rates of variable energy generation while maintaining voltage and frequency levels in the allowable range at the Point of Common

Coupling (PCC). Hence, mitigating solutions should be addressed for enhancing the power quality indexes and providing support during fault conditions.

Power generation from waves has been studied since the 1970s [4]. Nevertheless, no mature technology to extract this energy and produce electricity has been developed yet. An overview of the different developed devices, known as wave energy converters (WECs), is presented in [5]. In particular, the commercial maturity of WECs is faced with obstacle of their complex integration into the grid due to the high intrinsic variability of waves [6].

A promising solution to mitigate RES non-programmable power generation consists of coupling energy storage systems (ESSs) with renewable-based power plants. ESSs allow one to meet the level of power quality for the generation side, as well as the reliability required by the demand side, due to high flexibility, efficiency, scalability, and affordability [7]. Additionally, ESSs are able to provide peak-shaving functionality and emergency power towards the grid when required. Consequently, ESS integration into RESs gives additional flexibility in enhancing RES penetration in the near future. Several storage technologies, such as flywheels, batteries, and supercapacitors, have been investigated in the literature in such a framework.

Concerning flywheel energy storage systems (FESSs), their integration into a wave farm is addressed in [8], which was aimed at the implementation of a new control strategy for power smoothing. A reduction in grid losses by 51% was achieved, improving the energy efficiency of the power network. Moreover, the integration of FESSs into a WEC plant achieved a reduction of 50% in power oscillations [9], covering 85% of the frequency excursions at the grid, based on real power generation profiles delivered to the electric grid. Another noteworthy study employed an FESS to enhance the dynamic stability of an integrated offshore wind and marine-current farm [10], while [11] proposes an interesting study concerning FESS application for wave power leveling. Among the several ESS technologies for power smoothing, supercapacitors (SCs) have also been analyzed [12,13]. SCs are characterized by high power densities (>5 kW/kg) with low specific energies (up to 5–10 Wh/kg), no hysteresis, an extremely high lifespan (>500,000 cycles), high daily self-discharge rates, and capital costs per kWh (about 75,000 USD/kWh) [14].

Battery energy storage systems (BESSs) represent the mainstream of ESS technologies to date, thanks to high energy density, scalability, flexibility, and efficiency [15–17]. Nevertheless, being electrochemical devices, Li-ion batteries are subjected to degradation, being strongly affected by harmful power spikes and deep depths of discharge (DoDs). Therefore, many replacements would be needed when BESSs are employed to absorb or provide instantaneous high-power spikes typical of wave energy. To avoid needing excessively sized BESSs for such applications, hybridization with short-term ESSs (such as flywheels and supercapacitors (SCs) characterized by high power-to-capacity ratios) should be carried out, with SCs and FESSs being dedicated to managing high power spikes, reducing the stresses on the complementary energy-intensive device, as performed in [14]. Moreover, the hybridization of complementary energy storage technologies can overcome the intrinsic limits of the single devices, widely extending the operating range over several conditions and different timeframes [18].

Coupling hybrid energy storage systems (HESSs) with renewable energy sources has been widely investigated in the scientific literature. For instance, several studies on HESS integration with PV and wind power plants, as well as onboard HESS installations, and their power management control are presented in the following studies. Ref. [19] proposes a battery–supercapacitor hybrid energy storage system for a more electric aircraft including a simple power management strategy based on discrete wavelet transform. In ref. [20], a super magnetic energy storage is coupled to a battery for Conditioning Outputs from Direct Drive Linear Wave Energy Converters. An SC–battery HESS with a suitable power management strategy is presented by the authors in [21] to recover energy from regenerative actuators installed in an aircraft. For stationary applications, an active power control for a hybrid photovoltaic (PV)–battery/supercapacitor system is proposed in [22], while probabilistic forecasting-based sizing and control are illustrated in [23]. As

regards power smoothing, ref. [24] shows a controller for a PV plant including a HESS that contains two layers: the first predicts the next day's irradiance profile and uses a clear-sky model to identify the cloud class, setting the initial values of the filter time constants for cloudy, moderate, and mild days, while the second layer adjusts the initial filter time constant based on the current power ramp rate sharing power to the HESS. In [25], a power management method that secures the preset state-of-charge range of a battery and SC to smooth power fluctuations with renewables using the virtual capacity concept of an energy storage system (ESS), by extending the SOC usage range, is proposed. Furthermore, [26] illustrates a method based on the improved moving average and ensemble empirical mode decomposition for wind power smoothing with the purpose of finding the HESS's optimal capacity configuration, while [27] implements an efficient energy management structure for a grid-connected PV system combined with a supercapacitor–battery HESS.

Nevertheless, even though the literature deals with energy storage integration, as in [20] for the conditioning of outputs from direct-drive linear WECs, only few research works address HESS integration into WECs. Specifically, a battery/ultra-capacitor HESS for smoothing the power of oscillating wave energy was investigated in [28], assessing the HESS's impact in terms of the minimization of the grid side converter rating. Improved grid stability and cost-effectiveness for the HESS solution compared to battery and supercapacitor non-hybrid solutions were the main outcomes. Ref. [29] implemented coordinated and stable control for a battery–flywheel HESS to avoid power fluctuations during the grid-connected operation of a wave generator. The study assessed voltage and frequency stability in grid-connected mode, giving no quantitative information regarding power oscillation reduction at the grid interface.

To fill this gap, this paper analyzes the benefits of Li-ion battery–supercapacitor HESS integration into a WEC, aiming at smoothing power oscillations produced by the WEC system and delivered to the grid. Similarly to a previous paper by the authors [30], a sizing procedure targeting specific performance indexes, rather than sizing features, is implemented, making this approach innovative with respect to the state of the art. Moreover, with respect to [30], which relates to a mini-grid application, suitable indexes are here defined in reference to the power-smoothing performance to be targeted by the HESS coupled to the WEC plant. A suitable multi-objective data-driven power management strategy, based on the simultaneous perturbation stochastic approximation (SPSA) algorithm, is implemented, aiming to minimize power fluctuations at the Point of Common Coupling (PCC). Moreover, by means of this strategy, a suitable sizing procedure is developed based on quantifying the reduction in terms of power ramp (defined as the power variation between two consecutive values over a 1 s time step) at the grid interface and at the battery terminals; thus, fixing these two indexes' values, the HESS's sizing can be determined.

Hence, the main aim and innovation introduced by this research are to demonstrate how a Li-ion battery–SC HESS and real-time stochastic power management strategy can hugely improve power quality at the PCC with the grid. Indeed, in this paper, a power oscillation reduction of over 70% is obtained with respect to the WEC generation profile in the case of the HESS coupling to the WEC, together with the implemented SPSA power management strategy. Moreover, the Li-ion battery is 25% less stressed thanks to the presence of supercapacitor, contributing to enhancing its lifespan. Results are obtained from dynamic simulations carried out in a MATLAB®/Simulink R2023a environment considering three different wave power profiles, each one related to a specific real site located in the European region.

The paper is organized as follows: Section 2 illustrates the implemented methodology relating to the system modeling, power management strategy, and HESS sizing, while Section 3 reports the main outcomes of the simulations.

2. Methodology

In this section, the implemented methodology is described, from the statistical characterization of the input data to the system dynamic modeling and the HESS sizing.

2.1. Statistical Analysis on Input Data

The considered wave power profiles were gathered from thirty-year wave hindcast data validated through experimental measurements, as described in [31]. The hindcast was performed using the National Oceanic and Atmospheric Administration WAVEWATCH III model data and was driven by winds from the NCEP Climate Forecast System Reanalysis (CFSR), a reanalysis of atmospheric, oceanic, sea ice, and land data. Three sites in the European region were taken into account (located in France, England, and Norway). Specifically, an annual mean wave power ranging between 30 and 50 kW/m was registered for the three sites.

The actual wave occurrences of each one of the three considered sites were elaborated as yearly scatter matrices by means of aggregating the samples with the same wave height, Hs, and period, Tp. The resulting number of sea states are as follows:

- Site 1 (France): 143 sea states;
- Site 2 (England): 144 sea states;
- Site 3 (Norway): 132 sea states.

An Oscillating Wave Surge Converter (OWSC) was considered as the WEC technology. Specifically, it is composed of two PTOs each with 250 kW as their rated power. Figure 1 illustrates the OWSC layout. According to [32], a WEC is composed of:

- The prime mover, which absorbs wave power and transfers forces and motions to the reaction and power take-off subsystems through suitable connections.
- The power take-off (PTO) subsystem converting the wave energy extracted by the prime mover into electricity.
- The reaction subsystem that anchors the WEC to the seabed, providing a reaction point for the PTO and/or support for the hydrodynamic subsystem(s).
- The control and monitoring subsystem, dedicated to the WEC's control and management. It is composed of control software, sensors, and devices for data transferring.
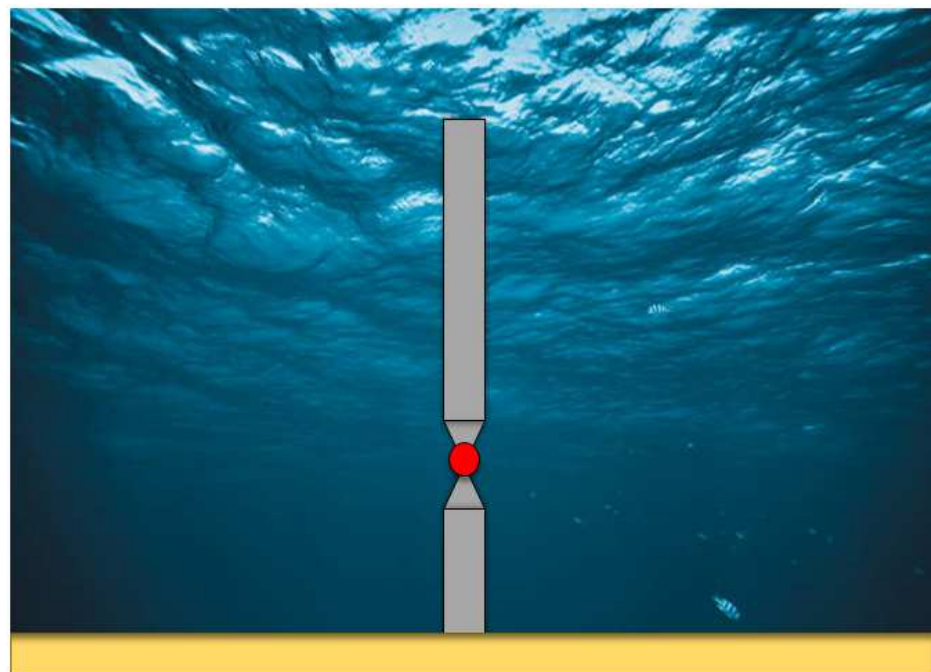

Figure 1. Schematic view of the Oscillating Wave Surge Converter (OWSC).

The implemented procedure for the generation of the three annual power profiles with a time step of 0.1 s and the subsequent statistical analysis for the selection of the most representative days is described in detail in a previous work by the authors [31]. In

detail, such daily profiles (with a 1 s time step) to be implemented in the simulations were extracted from the yearly profile according to the following criteria:

- Day 1, the day with the maximum power bandwidth (i.e., defined as the difference between the maximum and minimum power value over the day).
- Day 2, the day with the maximum mean power.
- Day 3, the day with the maximum bandwidth-to-mean-power ratio (i.e., the difference between the maximum bandwidth as defined above and the mean power over the day).
- Day 4, the day with the minimum bandwidth-to-mean-power ratio.
- Day 5, the day with the maximum mean power ramp.

Such selected criteria cover a wide range of power variations for the studied cases [31]. To highlight the different power distribution features for the three sites, Table 1 lists the average value and standard deviation for (i) power bandwidth and (ii) maximum bandwidth-to-mean-power ratio, both assessed on a yearly basis. Furthermore, it details the mean and minimum/maximum values in reference to the power ramp and power at each installation site.

Table 1. Power distribution statistics of the three considered sites.

	Site 1		Site 2		Site 3	
	μ	σ	μ	σ	μ	σ
Bandwidth (kW)	399	5	397	10	400	0.5
Maximum bandwidth-to-mean-power ratio (-)	13.2	1.8	18	2.7	12.6	2.2
	μ	min/max	μ	min/max	μ	min/max
Power ramp (kW/s)	2.8	0–7.5	2.1	0–6.3	3	0–8
Power (kW)	31	0–81	22	0–66	32	0–86

2.2. Stochastic Power Management Strategy: Theory and Implementation

The stochastic nature of renewables involves a high degree of complexity due to the management of non-programmable power generation. This becomes more challenging when the power management has to compute the power share among renewable sources, hybrid storage devices, and the grid efficiently and in real time. Therefore, an efficient power management strategy needs suitable optimization algorithms [33].

Several algorithms, such as linear, non-linear, dynamic, and stochastic algorithms, are proposed in the scientific literature to minimize several parameters, such as emissions or costs. Recently, artificial intelligence techniques and hybrid algorithms have gained attention for being applicable to non-linear problems [34].

Nonetheless, convergence issues and dependence on the initial estimate of the solution constitute key drawbacks for the application of artificial intelligence to real-time optimization problems.

To overcome such issues, multivariate stochastic optimization can be an efficient and effective solution in the control of several engineering systems, as indicated in [35]. Stochastic algorithms, including linear ones, are considered gradient based optimization approaches, as in the case of the SPSA algorithm and Lyapunov technique, that show the highest potential for real-time power management strategy implementation. Both the SPSA and Lyapunov techniques can operate with no knowledge of the future, requiring no mathematical uncertainty models or consideration of forecast errors [36]. Moreover, they allow multi-objective formulations, but SPSA shows advantages such as global optimum determination, easier performance function selection, and lower computational burden. Therefore, SPSA, recently proposed by the authors of [31,33,37], is worthy of further investigation for real-time power management applications of HESSs coupled to RES plants over a wide range of installed power. The SPSA algorithm, first introduced by Spall in 1992, represents a fast convergent alternative for the global optimization problem of an unknown functional form of system performance, defined as the loss function [38]. SPSA

is characterized by robustness to noise in loss measurements, ease of implementation, no necessity for a loss function gradient, and an ability to find the global minimum, making this algorithm suitable for a wide range of applications [39–43].

The mathematical formulation of SPSA starts from an initial estimation of the parameter vector ($\hat{\theta}$), through which the algorithm determines the optimal solution through iterations, by means of the simultaneous perturbation of all parameters within the current estimate. The algorithm parameters are updated for each iteration, as detailed by Equations (1) and (2). The values of the parameters a, c, α, γ are chosen to guarantee algorithm convergence [32,35].

$$a_k = \frac{a}{(A + k + 1)^\alpha} \tag{1}$$

$$c_k = \frac{c}{(k + 1)^\gamma} \tag{2}$$

Two different estimates of the vector $\hat{\theta}$ are computed, through the perturbation of the current estimation, as expressed by Equation (3). In detail, the elements of the perturbation vector (Δ_k) follow a Bernoulli distribution, as reported in [39].

$$\hat{\theta}_k^\pm = \hat{\theta} \pm c_k \Delta_k \tag{3}$$

The solution of the optimization problem produces a vector of parameters that minimizes the gradient of the loss function. The estimate of $\hat{g}(\hat{\theta})$ at the kth iteration is computed as expressed in Equation (4), where $\Delta_k \in \mathbb{R}^p$ represents a vector of p mutually independent mean zero random variables.

$$\hat{g}_k(\hat{\theta}_k) = \frac{\partial L_k}{\partial \theta_k} = \frac{y(\hat{\theta}_k^+) - y(\hat{\theta}_k^-)}{2c_k} \begin{bmatrix} \Delta_{k1}^{-1} \\ \Delta_{k2}^{-1} \\ \dots \\ \Delta_{kp}^{-1} \end{bmatrix} \tag{4}$$

To conclude, the current estimate is updated by means of Equation (5), and the loss function is re-evaluated.

$$\hat{\theta}_{k+1} = \hat{\theta}_k - a_k \hat{g}_k(\hat{\theta}_k) \tag{5}$$

The iterative process ends once either the convergence condition or the maximum number of iterations is reached. Specifically, the SPSA power management strategy was executed as follows. The vector of unknown parameters (θ) was composed of three dimensionless shares (i.e., Li-ion battery, supercapacitor, and grid, namely q_{BATT}, q_{SC}, and q_{GRID}), as reported in Equation (6).

$$\theta = \begin{bmatrix} q_{BATT} \\ q_{SC} \\ q_{GRID} \end{bmatrix} \tag{6}$$

Consequently, the split power values were calculated according to (7).

$$\begin{cases} P_{BATT} = q_{BATT} \Delta P \\ P_{SC} = q_{SC} \Delta P \\ P_{GRID} = q_{GRID} \Delta P \end{cases} \tag{7}$$

where $\Delta P = P_{wave}^t - P_{grid}^{t-1}(W)$ is defined as the difference between the wave power generation at time t and the grid power at the previous instant ($t - 1$). The SPSA parameters were chosen in accordance with [37].

The power shares were instantaneously assigned to the considered components, aiming at pursuing the following objectives:

1. Smooth the grid power profile by means of the ratio between the power delivered to the grid at timestep t and the power delivered at the previous instant ($t - 1$), as described by (8).

$$y_1^t(\theta) = \left(\frac{q_{GRID}\Delta P}{P_{GRID}^{t-1}} \right)^2 \tag{8}$$

2. Smooth the Li-ion battery-managed power profile by means of the ratio between the battery power at timestep t and the one at the previous instant ($t - 1$), as expressed by (9).

$$y_2^t(\theta) = \left(\frac{q_{BATT}\Delta P}{P_{BATT}^{t-1}} \right)^2 \tag{9}$$

Equation (10) models the multi-objective problem via the weighted sum of such objectives, accounting for the SPSA algorithm loss function.

$$y^t(\theta) = w_1 y_1^t(\theta) + w_2 y_2^t(\theta) \tag{10}$$

The two weights w_1 and w_2 were equally set to 0.5. The initial estimate of the vector θ was computed according to (11).

$$\theta = \begin{bmatrix} 0.7 \\ 0.02 \\ 0.28 \end{bmatrix} \tag{11}$$

2.3. Dynamic Modeling of the System

A dynamic model was developed in the MATLAB/Simulink environment to study and analyze the instantaneous power interactions among the WEC, the HESS, and the grid. This was to assess the performance of the SPSA power management strategy in terms of the power-smoothing effect towards the grid. The time step of the simulations was set as equal to 1 s. Figure 2 illustrates the model schematic layout, consisting of the following:

- The instantaneous daily power profile generated by the WEC, used as the input for computing the optimal power shares in the power management section.
- The power management strategy, based on the SPSA algorithm, which instantaneously controls the power shares among the components and the grid, taking into account the power ramp values at the previous step and the HESS technical features and states of charge.
- The HESS module composed of two subsystems related to the Li-ion battery pack and supercapacitor pack, respectively. The battery and supercapacitor implementation in the model are described in the following paragraphs.
- The grid.
- Li-Ion Battery

The battery dynamic model, tuned according to the technical specifications deduced from [44], was implemented according to [21]. Specifically, the open-circuit voltage (V_{ocv}) and internal resistance (R_{bat}^{int}) for charge and discharge were collected from through experimental tests on LFP cells.

Battery current (I_{bat}) and voltage (V_{bat}) can be determined according to Equations (12) and (13):

$$I_{bat} = \frac{V_{ocv} - \sqrt{V_{ocv}^2 - 4R_{bat}^{int}}}{2R_{bat}^{int}} \tag{12}$$

$$V_{bat} = V_{ocv} - R_{bat}^{int_{bat}} \tag{13}$$

where P represents the instantaneous power managed by the battery (in W) and

$$V_{ocv} = \left\{ \begin{array}{ll} V_{ocv,c} = f_1(SOC_{bat}) & \text{charge} \\ V_{ocv,d} = f_2(SOC_{bat}) & \text{discharge} \end{array} \right\} \tag{14}$$

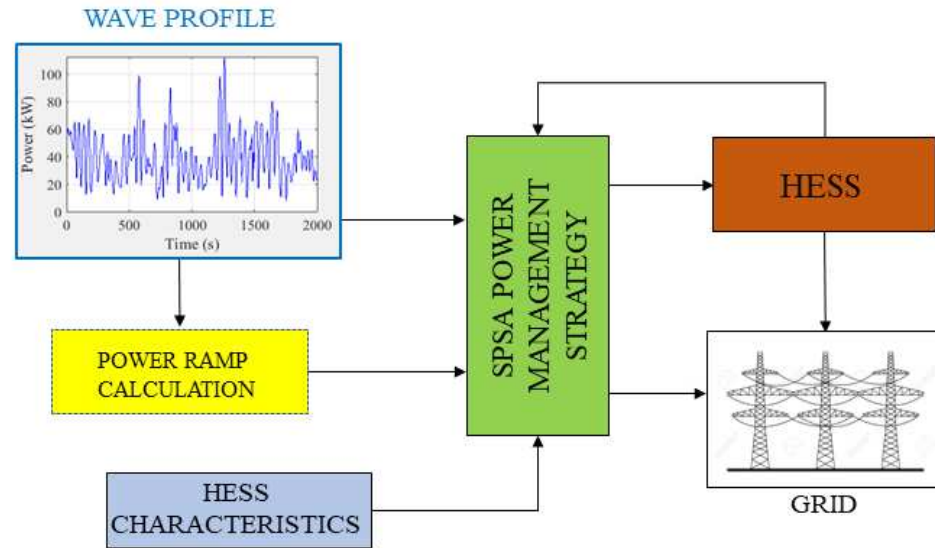$$R_{bat}^{int} = \left\{ \begin{array}{ll} R_{ch} = f_3(SOC_{bat}) & \text{charge} \\ R_{dis} = f_4(SOC_{bat}) & \text{discharge} \end{array} \right\} \tag{15}$$

Figure 2. Schematic layout of the model implemented in MATLAB/Simulink.

Equations (14) and (15) were implemented in the model through look-up tables on the basis of the experimental data obtained by the authors on LFP cells. The instantaneous SOC_{bat} was computed as expressed by Equations (16) and (17):

$$SOC_{bat} = SOC_{bat,ini} - \int \frac{\eta I_{bat}}{Q} \tag{16}$$

$$\eta = \left\{ \begin{array}{ll} \eta_{ch} = \frac{V_{ocv}}{V_{ocv} - I_{bat}R_{ch}} & \text{charge} \\ \eta_{dis} = \frac{V_{ocv} - I_{bat}R_{dis}}{V_{ocv}} & \text{discharge} \end{array} \right\} \tag{17}$$

where $SOC_{bat,ini}$ is the initial value of SOC_{bat} and Q (Ah) is the battery capacity. A battery round-trip efficiency of 90% was set.

- Supercapacitor

The supercapacitor section was developed referring to its equivalent circuit, presented in [21]. The instantaneous power at the previous step, managed by the supercapacitor, represents the SC model input. The SC section gives the following as outputs:

- The SC state of charge current value (SOC_{cap}), obtained as the ratio between the integral of the current i_{sc} and the charge nominal value (Q_{nom}).
- The actual instantaneous power managed by the SC.

Specifically, a two-branch equivalent circuit model, shown in Figure 3, was selected.

The equivalent circuit is composed of two branches, i.e., the "main cell" branch and the "slow cell" branch. The "main cell" identifies SC fast charging/discharging processes (order of seconds). The series resistance R_1 represents the heat loss during the SC operation and it is measured in mΩ. The capacitor C_1 (F) is a function of the voltage V_1 (Equation (18)), where C_0 is the constant capacitance measured in Farad (F) and C_v is a constant parameter expressed in (F V^{-1}).
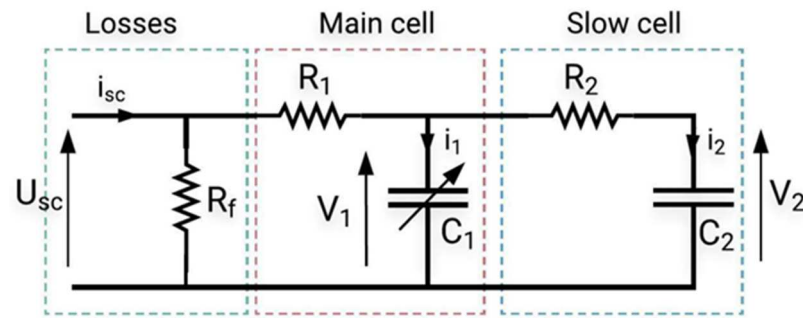
$$C_1 = C_0 + C_v V_1 \tag{18}$$

Figure 3. Two-branch equivalent model of the supercapacitor (from [21]).

On the other hand, the "slow cell" branch defines the internal energy distribution at the end of the charge or discharge process (range of minutes). The parallel resistance R_f defines the leakage current when the SC is in stand-by mode (10^2 kΩ). The voltage V_2 relative to the "slow cell" branch is calculated by Equation (19):

$$V_2 = \frac{1}{C_2} \int \frac{1}{R_2}(V_1 - V_2)dt \tag{19}$$

where C_2 and R_2 are the capacitance (F) and the resistance (Ω) of the "slow cell". As specified in [21], the "slow cell" can be neglected when only the fast discharge/charge cycles are considered. Equation (20) shows the voltage, V_{sc}, of the SC module, considering the number of series (N_s) and parallel (N_p) electrically connected SC cells.

$$V_{sc} = N_s U_{sc} = N_s \left(V_1 + R_1 \frac{I_{sc}}{N_p} \right) \tag{20}$$

Moreover, U_{sc} and I_{sc} represent the current and voltage of the single cell, respectively. Therefore, the voltage V_1 across the capacitor C_1 can be calculated by Equation (21).

$$V_1 = \frac{-C_0 + \sqrt{C_0^2 + 2C_v Q_1}}{C_v} \tag{21}$$

where Q_1 is the instantaneous charge of the capacitor C_1, determined by Equation (22).

$$Q_1 = C_0 V_1 + \frac{1}{2} C_v V_1^2 \tag{22}$$

Specifically, the supercapacitor pack consists of several supercapacitors characterized by a capacitance of 650 F and a peak power of 1 kW. The specification of the selected SC can be found in [45]. Since an SC does not involve electrochemical reactions, no degradation issues are caused by deep discharge; therefore, a depth of discharge (DoD) of 100% was set. The operating voltage falls within 1.35–2.7 V [46].

The SC characteristic parameters to be implemented in the model were obtained by a linear interpolation on experimental data deduced from two different supercapacitors [21], respectively, with a lower and a higher capacity with respect to the selected one. Table 2 lists the equivalent parameters of the supercapacitor cell.

Table 2. Equivalent parameters of the considered Maxwell BCAP0650 supercapacitor.

SC Equivalent Parameters	
R_1	2.33 mΩ
C_0	380 F
C_v	262 F V^{-1}
R_2	0.8126 Ω
C_2	117 F
V_{rated}	2.7 V
V_{max}	2.85 V
C_{rated}	650 F
P_{max}	1 kW
Cell weight	0.16 kg

2.4. Sizing Procedure of the Hybrid Energy Storage System

The sizing procedure moved from the Cumulative Density Functions (CDFs) of power ramp profiles (assessed over a 1 s time step) at the grid, WEC, battery, and SC terminals determined through the model (see Section 2.3) simulation for different investigated days and installation sites. In detail, battery sizing was chosen as determined in [31] for coupling with the same WECs in the three considered sites, while the supercapacitor device was sized to reach the following conditions:

1. With respect to the fluctuation at the WEC terminals, an average instantaneous percentage reduction in the power rate sent to the grid of at least −70% among all the considered days for the specific site, as expressed by Equation (23):

$$Grid \ to \ WEC \ (\%) = \frac{PR_{GRID} - PR_{WEC}}{PR_{WEC}} \leq -70\% \tag{23}$$

   where PR_{GRID} and PR_{WEC} represent the power ramp values, in W/s, assessed at an 80% CDF threshold for the grid and WEC power ramp, respectively.

2. With respect to the SC's absence, an average instantaneous percentage reduction in the power ramp managed by the battery was targeted thanks to the SC smoothing effect. Specifically, the power ramp managed by the SC was fixed to be equal to at least 25% of the total power ramp managed by the HESS among all the considered days for the specific site, as expressed by Equation (24):

$$SCtoBatt(\%) = \frac{-PR_{SC}}{PR_{BATT} + PR_{SC}} \leq -25\% \tag{24}$$

   where PR_{SC} and PR_{BATT} represent the power ramp values, in W/s, assessed at an 80% CDF threshold for the supercapacitor and battery, respectively.

The sizing procedure was as follows: starting from the final sizing determined in a previous work by the authors [31], 24 kWh was considered as the Li-ion battery nominal capacity (discharge/charge rates of 3C and 1C, respectively). Simulations were performed for all the selected days of all three considered sites, moving from the case of the 24 kWh Li-ion battery with a very low number of SCs electrically placed in parallel (i.e., 10 SC cells). The simulations' outcomes were then post-processed, evaluating the power ramps managed by the battery, the SC, and the grid. Subsequently, these trends were cumulated and the PR_{GRID}, PR_{SC}, and PR_{BATT} values were assessed at 80% CDF. The satisfaction of Equations (23) and (24) was therefore evaluated with reference to the values obtained. The capacity of the SC was increased until the conditions set in relation to both indices were satisfied (Equations (23) and (24)), by means of increasing the number of SC units in parallel, with a step equal to 10 units per cycle. Table 3 lists the nominal power and capacity of the final HESS sizing.

Table 3. Final sizing of the HESS devices.

	Site 1–Site 2–Site 3		
	Total Cell Number	**Power [kw]**	**Capacity [kWh]**
Supercapacitor	60 parallel	65.3	0.026
Li-ion battery	100 series	72	24

3. Results and Discussion

According to the sizing procedure, the power-smoothing effect of the SPSA power management strategy on the grid was evaluated for all three sites.

Figures 4–6 illustrate the main outcomes of the simulation. Specifically, the power fluctuations registered at the grid interface were strongly reduced with respect to the wave power generation in all three sites. Moreover, the battery and supercapacitor SoCs and powers are reported to show the benefits of HESS integration for smoothing the power fluctuations at the PCC. In detail, it is highlighted that the Li-ion battery SoC (depicted by the red dotted line) did not significantly vary thanks to the supercapacitor peak-shaving function, whose SoC variation is represented by the blue dotted line. This feature allows reduced battery power stress, contributing to extending its lifespan. Moreover, the power oscillations sent at the PCC (represented by the black solid line) were strongly reduced for all the studied days relating to all the three sites.
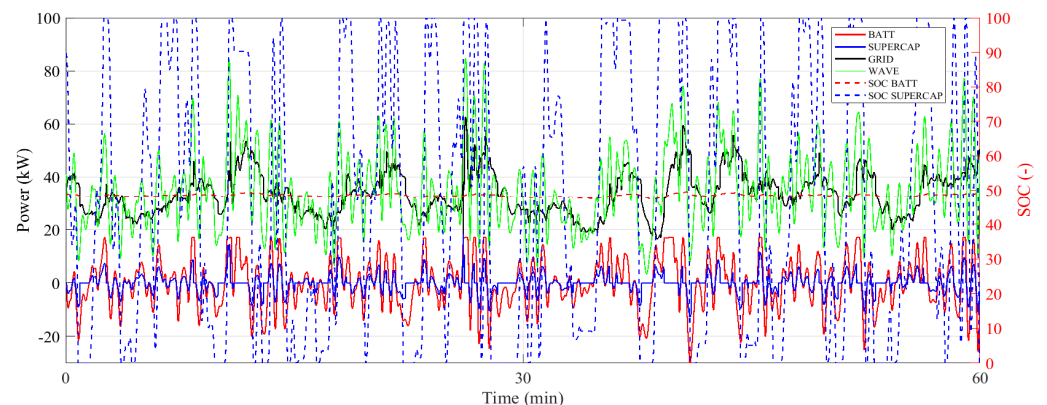

Figure 4. One-hour simulation instantaneous parameters relating to day 1 (site 1) for battery (power—red solid line, SoC—red dotted line), supercapacitor (power—blue solid line, SoC—blue dotted line), grid power (black solid line), and wave power generation (green solid line). Battery and supercapacitor negative power values correspond to discharge, while positive values correspond to charge.

To quantify the power-smoothing effect, the power fluctuation achieved at the PCC, thanks to coupling the HESS with wave energy converters and the implemented stochastic power management algorithm, was considered. The assessment was carried out considering 80% as the threshold value for the CDF of the power at the PCC. The benefits of HESS integration were also assessed in terms of the battery power ramp reduction thanks to the SC's presence. As detailed in the sizing procedure and considering the implemented SPSA power management strategy, the SC pack was sized to manage at least 25% of the overall fluctuation at the HESS terminals. Covering a wide range of WEC operating modes through an accurate statistical selection of the simulated days, it is noteworthy that the simulation outcomes listed in Tables 4–6 and depicted in Figures 7–9 exhibit the same performances for all the considered days and sites. This demonstrates that battery–supercapacitor HESS integration with a highly variable renewable energy source such as wave energy, together with a customized data-driven SPSA power management strategy, improves the power injected into the grid, contributing to the stability and safety of grid provision. Specifically,

Tables 4–6 illustrate the values of the power ramps at 80% CDF for all the days of the three considered sites. Moreover, the grid-to-WEC and the supercapacitor-to-battery power ramp reductions are also listed, demonstrating the benefits of coupling the HESS to the WEC in terms of both power smoothing and a reduction in battery stress thanks to SC operation.
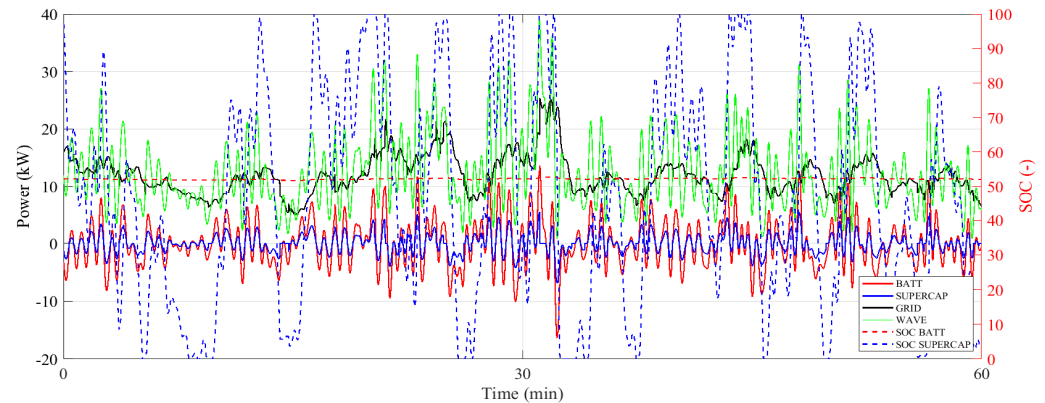

Figure 5. One-hour simulation instantaneous parameters relating to day 3 (site 2) for battery (power—red solid line, SoC—red dotted line), supercapacitor (power—blue solid line, SoC—blue dotted line), grid power (black solid line), and wave power generation (green solid line). Battery and supercapacitor negative power values correspond to discharge, while positive values correspond to charge.
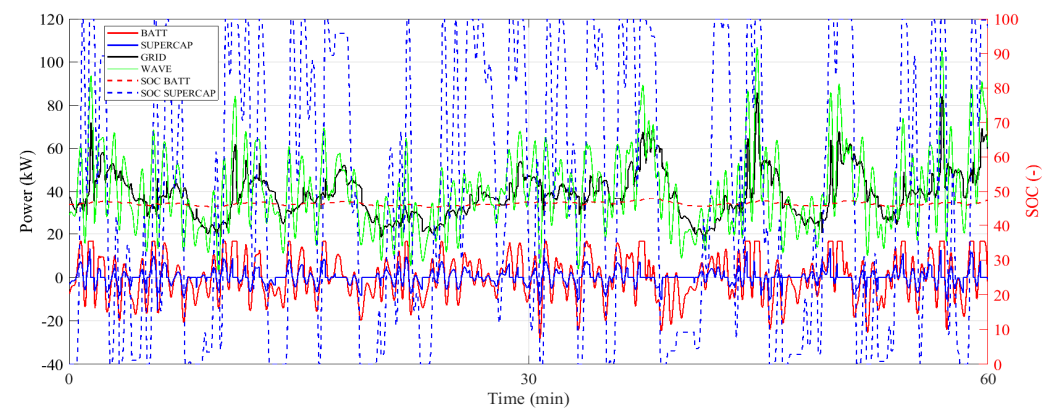

Figure 6. One-hour simulation instantaneous parameters relating to day 5 (site 3) for battery (power—red solid line, SoC—red dotted line), supercapacitor (power—blue solid line, SoC—blue dotted line), grid power (black solid line), and wave power generation (green solid line). Battery and supercapacitor negative power values correspond to discharge, while positive values correspond to charge.

**Table 4.** Power ramp values obtained from simulations in reference to the final HESS sizing at 80% CDF for site 1.

	PR_{batt} (W/s)	PR_{sc} (W/s)	PR_{WEC} (W/s)	PR_{grid} (W/s)
Day 1	1788	640	2487	739
Day 2	1941	681	2732	840
Day 3	1022	378	1404	345
Day 4	1338	476	1839	480
Day 5	1941	681	2732	840

Table 5. Power ramp values obtained from simulations in reference to the final HESS sizing at 80% CDF for site 2.

	PR$_{batt}$ (W/s)	PR$_{sc}$ (W/s)	PR$_{WEC}$ (W/s)	PR$_{grid}$ (W/s)
Day 1	1493	546	2104	573
Day 2	1650	590	2314	609
Day 3	835	320	1153	267
Day 4	1280	468	1767	439
Day 5	1650	590	2314	609

Table 6. Power ramp values obtained from simulations in reference to the final HESS sizing at 80% CDF for site 3.

	PR$_{batt}$ (W/s)	PR$_{sc}$ (W/s)	PR$_{WEC}$ (W/s)	PR$_{grid}$ (W/s)
Day 1	1640	594	2278	678
Day 2	2300	818	3292	1063
Day 3	1048	391	1451	337
Day 4	1633	592	2256	642
Day 5	2300	818	3292	1063
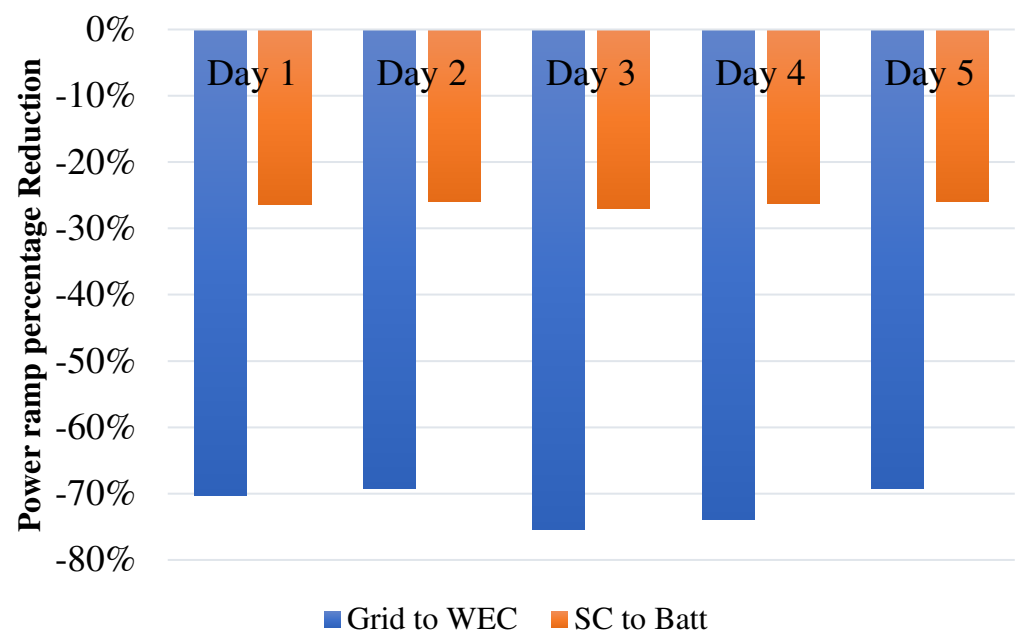
Figure 7. Assessment of grid power ramp reduction with respect to wave generation and battery power ramp reduction due to the presence of the supercapacitor for all the days at site 1.
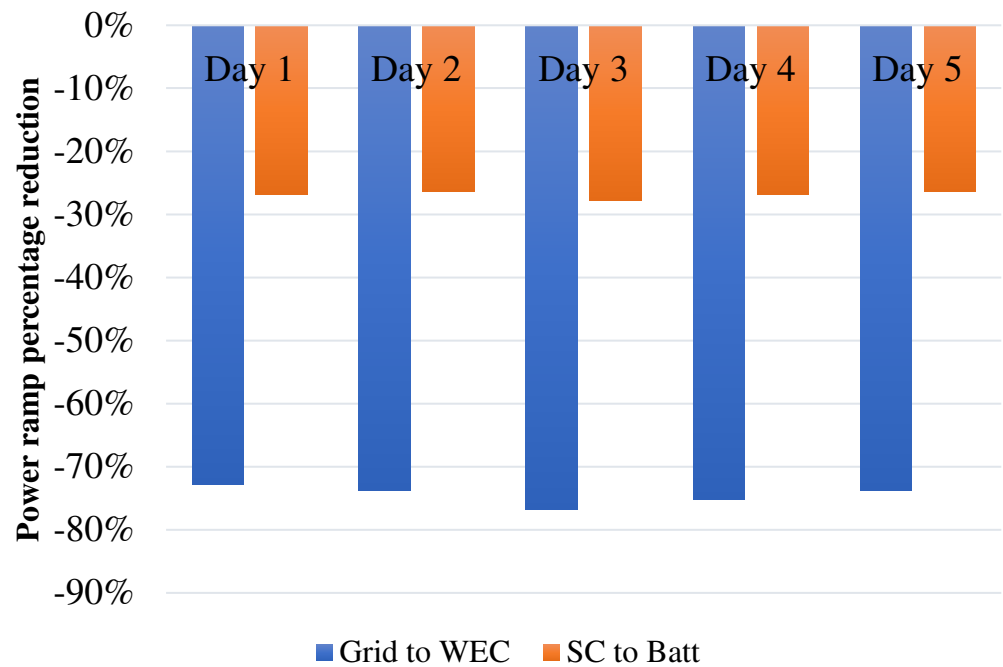
Figure 8. Assessment of grid power ramp reduction with respect to wave generation and battery power ramp reduction due to the presence of the supercapacitor for all the days at site 2.

Figure 9. Assessment of grid power ramp reduction with respect to wave generation and battery power ramp reduction due to the presence of the supercapacitor for all the days at site 3.
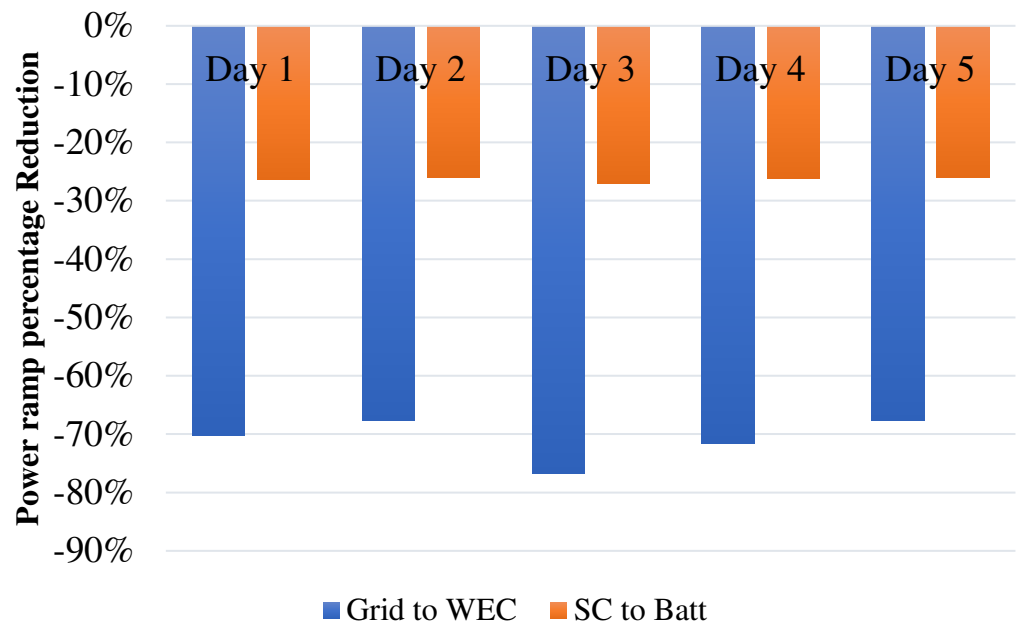
4. Conclusions

Wave energy is currently widely investigated since it has a very high theoretical potential. Although wave power generation is extremely fluctuating and intermittent, no WEC technology represents the mainstream to date. Therefore, research efforts address enhancing the efficiency of generation. Moreover, due to the stochastic nature of waves, one of the most significant issues is related to the grid connection of such devices. To overcome this issue, HESS integration represents a very effective and efficient solution to enhance grid power quality and stability. Here, a supercapacitor–Li-ion battery HESS is coupled to a WEC to perform output power smoothing at the PCC to maximize WEC

power production and reduce Li-ion battery stress. To implement this, a suitable power management strategy based on the SPSA algorithm for allocating the instantaneous power shares among the components and the grid is developed, allowing a reduction of more than 70% in the power oscillations at the grid interface. By means of the definition of two performance indexes relating to the grid power ramp and battery stress reductions, a proper HESS sizing procedure is carried out. In addition, the performed simulations demonstrate that the supercapacitor features act to extend the Li-ion battery's lifespan, reducing battery stress by more than 25% compared to a non-hybrid ESS only consisting of a Li-ion battery.

Author Contributions: Conceptualization, D.P. and L.B.; methodology, D.P. and L.B.; software, D.P.; validation, D.P. and L.B.; formal analysis, D.P.; investigation, D.P.; resources, L.B.; data provision, F.G. and G.A.; data curation, F.G., G.A. and D.P.; writing—original draft preparation, D.P. and L.B.; writing—review and editing, L.B.; visualization, D.P.; supervision, L.B.; project administration, L.B. All authors have read and agreed to the published version of the manuscript.

Data Availability Statement: Data are contained within the article.

Conflicts of Interest: F.G. and G.A. were employed by VGA srl. The remaining authors declare that the research was conducted in the absence of any commercial or financial relationships that could be construed as a potential conflict of interest.

References

1. IRENA. *Wave Energy Technology Brief*; IRENA: Masdar City, United Arab Emirates, 2014.
2. Data & Statistics—IEA. Available online: https://www.iea.org/data-and-statistics?country=WORLD&fuel=Energy%20 consumption&indicator=Electricity%20consumption (accessed on 21 September 2020).
3. Brahmendra Kumar, G.V.; Sarojini, R.K.; Palanisamy, K.; Padmanaban, S.; Holm-Nielsen, J.B. Large Scale Renewable Energy Integration: Issues and Solutions. *Energies* **2019**, *12*, 1996. [CrossRef]
4. Qiao, D.; Haider, R.; Yan, J.; Ning, D.; Li, B. Review of Wave Energy Converter and Design of Mooring System. *Sustainability* **2020**, *12*, 8251. [CrossRef]
5. Falcao, A.F.D.O. Wave Energy Utilization: A Review of the Technologies. *Renew. Sustain. Energy Rev.* **2010**, *14*, 899–918. [CrossRef]
6. Aderinto, T.; Li, H. Ocean Wave Energy Converters: Status and Challenges. *Energies* **2018**, *11*, 1250. [CrossRef]
7. Zahedi, A. Maximizing Solar PV Energy Penetration Using Energy Storage Technology. *Renew. Sustain. Energy Rev.* **2011**, *15*, 866–870. [CrossRef]
8. Rojas-Delgado, B.; Alonso, M.; Amaris, H.; De Santiago, J. Wave Power Output Smoothing through the Use of a High-Speed Kinetic Buffer. *Energies* **2019**, *12*, 2196. [CrossRef]
9. Torres, J.; Blanco, M.; Lafoz, M.; Navarro, G.; Nájera, J.; Santos-Herran, M. Dimensioning Methodology of Energy Storage Systems for Power Smoothing in a Wave Energy Conversion Plant Considering Efficiency Maps and Filtering Control Techniques. *Energies* **2020**, *13*, 3380. [CrossRef]
10. Wang, L.; Yu, J.Y.; Chen, Y.T. Dynamic Stability Improvement of an Integrated Offshore Wind and Marine-Current Farm Using a Flywheel Energy-Storage System. *IET Renew. Power Gener.* **2011**, *5*, 387–396. [CrossRef]
11. Yoshida, T.; Sanada, M.; Morimoto, S.; Inoue, Y. Study of Flywheel Energy Storage System for Power Leveling of Wave Power Generation System. In Proceedings of the ICEMS 2012—Proceedings: 15th International Conference on Electrical Machines and Systems, Sapporo, Japan, 21–24 October 2012; IEEE: Denver, CO, USA, 2012.
12. Moreno-Torres, P.; Blanco, M.; Navarro, G.; Lafoz, M. Power Smoothing System for Wave Energy Converters by Means of a Supercapacitor-Based Energy Storage System. In Proceedings of the 2015 17th European Conference on Power Electronics and Applications, EPE-ECCE Europe 2015, Geneva, Switzerland, 8–10 September 2015. Jointly owned by EPE Association and IEEE PELS.
13. Murray, D.B.; Egan, M.G.; Hayes, J.G.; Sullivan, D.L.O. Applications of Supercapacitor Energy Storage for a Wave Energy Converter System. In Proceedings of the Eighth European Wave and Tidal Energy Conference, Uppsala, Sweden, 7–9 September 2009; pp. 786–795.
14. Mongird, K.; Viswanathan, V.; Balducci, P.; Alam, J.; Fotedar, V.; Koritarov, V.; Hadjerioua, B. An Evaluation of Energy Storage Cost and Performance Characteristics. *Energies* **2020**, *13*, 3307. [CrossRef]

15. Pelosi, D.; Barelli, L.; Longo, M.; Zaninelli, D. Assessment Analysis of BEV/PHEV Recharge in a Residential Micro-Grid Based on Renewable Generation. In *Sustainability in Energy and Buildings 2022*; Littlewood, J., Howlett, R.J., Jain, L.C., Eds.; Springer Nature: Singapore, 2023; pp. 130–139.

16. Barelli, L.; Pelosi, D.; Longo, M.; Zaninelli, D. Energy Storage Integration into Fast Charging Stations Installed on E-Highways. In Proceedings of the 2022 IEEE Power & Energy Society General Meeting (PESGM), Denver, CO, USA, 17–21 July 2022; IEEE: Denver, CO, USA, 2022.

17. Pelosi, D.; Longo, M.; Bidini, G.; Zaninelli, D.; Barelli, L. A New Concept of Highways Infrastructure Integrating Energy Storage Devices for E-Mobility Transition. *J. Energy Storage* **2023**, *65*, 107364. [CrossRef]

18. Barelli, L.; Bidini, G.; Cherubini, P.; Micangeli, A.; Pelosi, D.; Tacconelli, C. How Hybridization of Energy Storage Technologies Can Provide Additional Flexibility and Competitiveness to Microgrids in the Context of Developing Countries. *Energies* **2019**, *12*, 3138. [CrossRef]

19. Cheng, L.; Zhang, F.; Liu, S.; Zhang, Z. Configuration Method of Hybrid Energy Storage System for High Power Density in More Electric Aircraft. *J. Power Sources* **2020**, *445*, 227322. [CrossRef]

20. Nie, Z.; Xiao, X.; Kang, Q.; Aggarwal, R.; Zhang, H.; Yuan, W. SMES-Battery Energy Storage System for Conditioning Outputs from Direct Drive Linear Wave Energy Converters. *IEEE Trans. Appl. Supercond.* **2013**, *23*, 5000705. [CrossRef]

21. Barelli, L.; Bidini, G.; Ottaviano, P.A.; Gallorini, F.; Pelosi, D. Coupling Hybrid Energy Storage System to Regenerative Actuators in a More Electric Aircraft: Dynamic Performance Analysis and CO_2 Emissions Assessment Concerning the Italian Regional Aviation Scenario. *J. Energy Storage* **2022**, *45*, 103776. [CrossRef]

22. Şahin, M.E.; Blaabjerg, F. A Hybrid PV-Battery/Supercapacitor System and a Basic Active Power Control Proposal in MATLAB/Simulink. *Electronics* **2020**, *9*, 129. [CrossRef]

23. Wan, C.; Qian, W.; Zhao, C.; Song, Y.; Yang, G. Probabilistic Forecasting Based Sizing and Control of Hybrid Energy Storage for Wind Power Smoothing. *IEEE Trans. Sustain. Energy* **2021**, *12*, 1841–1852. [CrossRef]

24. Abdalla, A.A.; El Moursi, M.S.; El-Fouly, T.H.; Hosani, K.H. Al A Novel Adaptive Power Smoothing Approach for PV Power Plant with Hybrid Energy Storage System. *IEEE Trans. Sustain. Energy* **2023**, *14*, 1457–1473. [CrossRef]

25. Nguyen, V.T.; Shim, J.W. Virtual Capacity of Hybrid Energy Storage Systems Using Adaptive State of Charge Range Control for Smoothing Renewable Intermittency. *IEEE Access* **2020**, *8*, 126951–126964. [CrossRef]

26. Yuming, C.; Peng, J.; Gaojun, M.; Yao, W.; Tiantian, L. Optimal Capacity Configuration of Hybrid Energy Storage System Considering Smoothing Wind Power Fluctuations and Economy. *IEEE Access* **2022**, *10*, 101229–101236. [CrossRef]

27. Bharatee, A.; Ray, P.K.; Ghosh, A. A Power Management Scheme for Grid-Connected PV Integrated with Hybrid Energy Storage System. *J. Mod. Power Syst. Clean Energy* **2022**, *10*, 954–963. [CrossRef]

28. Hazra, S.; Bhattacharya, S. Hybrid Energy Storage System Comprising of Battery and Ultra-Capacitor for Smoothing of Oscillating Wave Energy. In Proceedings of the ECCE 2016 IEEE Energy Conversion Congress and Exposition, Milwaukee, WI, USA, 18–22 September 2016; pp. 8–15. [CrossRef]

29. Fang, H.; Lin, S.; Chu, H.; Jia, T.; Liu, Y. Coordinated and Stable Control of a Hybrid Energy Storage System for Wave Generation System. In Proceedings of the World Congress on Intelligent Control and Automation (WCICA), Guilin, China, 12–15 June 2016; pp. 1986–1991.

30. Pelosi, D.; Baldinelli, A.; Cinti, G.; Ciupageanu, D.A.; Ottaviano, A.; Santori, F.; Carere, F.; Barelli, L. Battery-hydrogen vs. flywheel-battery hybrid storage systems for renewable energy integration in mini-grid: A techno-economic comparison. *J. Energy Storage* **2023**, *63*, 106968. [CrossRef]

31. Barelli, L.; Bidini, G.; Ciupageanu, D.A.; Ottaviano, A.; Pelosi, D.; Gallorini, F.; Alessandri, G.; Atcheson Cruz, M. An Effective Solution to Boost Generation from Waves: Benefits of a Hybrid Energy Storage System Integration to Wave Energy Converter in Grid-Connected Systems. *Open Res. Eur.* **2022**, *2*, 40. [CrossRef]

32. Pecher, A.; Kofoed, J.P. *Handbook of Ocean Wave Energy*; SpringerOpen: Berlin/Heidelberg, Germany, 2017; ISBN 9783319398884.

33. Barelli, L.; Bidini, G.; Ciupageanu, D.A.; Micangeli, A.; Ottaviano, P.A.; Pelosi, D. Real Time Power Management Strategy for Hybrid Energy Storage Systems Coupled with Variable Energy Sources in Power Smoothing Applications. *Energy Rep.* **2021**, *7*, 2872–2882. [CrossRef]

34. Neffati, A.; Guemri, M.; Caux, S.; Fadel, M. Energy Management Strategies for Multi Source Systems. *Electr. Power Syst. Res.* **2013**, *102*, 42–49. [CrossRef]

35. Byrne, R.H.; Nguyen, T.A.; Copp, D.A.; Chalamala, B.R.; Gyuk, I. Energy Management and Optimization Methods for Grid Energy Storage Systems. *IEEE Access* **2017**, *6*, 13231–13260. [CrossRef]

36. Ciupageanu, D.A.; Barelli, L.; Lazaroiu, G. Real-time stochastic power management strategies in hybrid renewable energy systems: A review of key applications and perspectives. *Electr. Power Syst. Res.* **2020**, *187*, 106497. [CrossRef]

37. Barelli, L.; Pelosi, D.; Ciupageanu, D.A.; Ottaviano, P.A.; Lazaroiu, G. Stochastic Power Management Strategy for Hybrid Energy Storage Systems to Enhance Large Scale Wind Energy Integration. *J. Energy Storage* **2020**, *31*, 101650. [CrossRef]

38. Spall, J.C. Multivariate Stochastic Approximation Using a Simultaneous Perturbation Gradient Approximation. *IEEE Trans. Autom. Contr.* **1992**, *37*, 332–341. [CrossRef]

39. Sadegh, P.; Spall, J.C. Optimal Random Perturbation for Stochastic Approximation Using a Simultaneous Perturbation Gradient Approximation. *IEEE Trans. Autom. Contr.* **1998**, *43*, 1480–1484. [CrossRef]

40. Spall, J.C. An Overview of the Simultaneous Perturbation Method. *Johns Hopkins APL Tech. Dig.* **1998**, *19*, 482–492.

41. Spall, J.C. A One-Measurement Form of Simultaneous Perturbation Stochastic Approximation. *Automatica* **1997**, *33*, 109–112. [CrossRef]
42. Ho, M.C.; Lim, J.M.-Y.; Chong, C.Y.; Chua, K.K.; Siah, A.K.L. High Dimensional Origin Destination Calibration Using Metamodel Assisted Simultaneous Perturbation Stochastic Approximation. *IEEE Trans. Intell. Transp. Syst.* **2023**, *24*, 3845–3854. [CrossRef]
43. Granichin, O.; Erofeeva, V.; Ivanskiy, Y.; Jiang, Y. Simultaneous Perturbation Stochastic Approximation-Based Consensus for Tracking under Unknown-But-Bounded Disturbances. *IEEE Trans. Automat. Contr.* **2021**, *66*, 3710–3717. [CrossRef]
44. GWL Power. *GB-LFP1865-11 Rechargeable Battery Datasheet*; GWL Power Ltd.: Prague, Czech Republic, 2016.
45. Maxwell Technologies. *2.7V 650-3000F Ultracapacitor Cells Datasheet*; Maxwell Technologies: San Diego, CA, USA, 2019.
46. Lahyani, A.; Venet, P.; Guermazi, A.; Troudi, A. Battery/Supercapacitors Combination in Uninterruptible Power Supply (UPS). *IEEE Trans. Power Electron.* **2013**, *28*, 1509–1522. [CrossRef]